

Investigating the Application and Impact of Laser Etching Technology in the Fabrication of Solar Cells

Zhao Wang, Guanggui Cheng,* Zigang Wang, Kuiyi Wu, Daming Chen, Yifeng Chen, Li Yin, Haixia Liu, Ningyi Yuan, Jifan Gao, and Jianning Ding*

The most crucial initial step in the metallization process of electroplating is the local contact openings in dielectric layers. In this article, an ultraviolet picosecond laser (UV-ps), is used to open the front and back dielectric layer of the precursor of n-TOPCon solar cells. By changing the laser parameters and spot overlap rate, the surface morphology of laser etching under different conditions is obtained and characterized by optical microscope and scanning electron microscope. The results indicate that there are three separate laser shock zones in the dielectric layer under the action of Gaussian light spot, and the corresponding ablation mechanisms are proposed. The longitudinal distribution of B element is characterized by secondary ion mass spectrometry to explore the effect of laser on its pn junction. In addition, the electrical characterization of lifetime photoluminescence is measured and calibrated using WCT120, and this indicates that the majority of the amorphous silicon is recrystallized when applying a fast firing oven process, and this hence improve the minority carrier lifetime and implied open-circuit voltage. The laser damage to the emitter at the laser-ablated regions is investigated using the emitter saturation current density, $J_{0\text{laser}}$ extracted by WCT120.

PV production,^[1] the metallization step is crucial interest. At present, screen printing (SP) is the main metallization technology for producing industrial silicon solar cells, which has the characteristics of simplicity, speed, and suitability for mass production. However, this method requires silver or silver-aluminum paste as the gate electrode, which is the most critical process and most expensive non silicon material used in current crystalline silicon (c-Si) cells.^[2,3] The n-TOPCon solar cells have higher light conversion efficiency than passivated emitter and rear cell (PERC) solar cells and can be compatible with PERC production lines. Due to the high silver consumption of n-TOPCon solar cells, it is necessary to find a method that can replace SP metallization and achieve the goal of reducing costs.

Nowadays, the main metallization methods that replace SP include laser transfer printing and electroplating (electrochemical deposition metallization). In this study, using Ni/Cu electroplating as a metallization technique not only reduces metal costs but also has the potential to overcome the limitations of SP (more dense contact, higher conductivity, better aspect ratio, narrower line width, lower contact resistance).^[4,5] **The most important step before electrochemical metallization is to selectively open the dielectric layer SiNx. Laser etching can meet this requirement. The technology not only meets the needs** of the laboratory but also enables reliable centralized mass production.^[6,7] Laser etching is a highly accurate non-contact method to open the dielectric layer and does not require the assistance of chemicals, reducing environmental pollution issues.

The choice of a laser should be dependent on the characteristics of the material, including its bandgap and reflectivity. Under no special circumstances, absorption takes place when the laser energy exceeds the bandgap of the material, and the converse is also true. Under high-intensity light, a number of photons are usually incident on the sample in a short period of time. The simultaneous absorption of multiple photons and high energy can exceed the bandgap of the material, leading to an increase in electron concentration in the conduction band.^[8] In recent years, laser ablation has also been used to form the contact openings of the front p-type emitter^[9,10] and rear of copper plated n-TOPCon solar cells. Grubel et al.^[11] used ultraviolet picosecond laser to open the front and back of n-TOPCon solar cells and then electroplated Ni/Cu on both sides.


1. Introduction

With the proposal of carbon neutrality, it is critical to develop renewable energies to meet future energy demand and limit global warming. Among the numerous new energy sources, solar cells are becoming increasingly mature and occupy an important proportion in the new energy industry. For silicon wafer photovoltaic (PV) technology, which accounts for 95% of the total solar

Z. Wang, G. Cheng, H. Liu, J. Ding
School of Materials Science and Engineering, Institute of Intelligent Flexible Mechatronics
Jiangsu University
Zhenjiang 212013, China
E-mail: ggcheng@ujs.edu.cn; dingjn@ujs.edu.cn

Z. Wang, Z. Wang, K. Wu, D. Chen, Y. Chen, L. Yin, J. Gao
State Key Lab of Photovoltaic Science and Technology
Trina Solar
Changzhou 213031, China

N. Yuan, J. Ding
Jiangsu Collaborative Innovation Center of Photovoltaic Science and Engineering
Changzhou University
Changzhou 213164, China

 The ORCID identification number(s) for the author(s) of this article can be found under <https://doi.org/10.1002/pssa.202300795>.

DOI: 10.1002/pssa.202300795

An optimized process sequence is developed and with this approach a solar cell efficiency of 22.5% is demonstrated on industrial bifacial TOPCon solar cells. Unoptimized laser parameters will lead to incomplete dielectric layer removal, serious pyramid melting on silicon surface, pn junction damage, defect increase, and so on. Laser damage to silicon solar cells and its impact on solar cell performance have been studied.^[12,13] Laser-induced damage can provide a pathway for copper diffusion, which means that optimization of laser parameters is critical to ensure the efficiency,^[14] pull-off force of the figures and busbars bonding,^[15] and component reliability of electroplated silicon solar cells.^[16,17]

In this article, we use UV-ps, with a pulse time of 10 ps, to investigate the burning mechanism of n-TOPCon solar cells and the effects of the laser process. Without considering other influencing factors, the defects caused by ultraviolet lasers are lighter than those caused by green and red light.

The price is lower than the femtosecond laser, the damage and thermal shock are lower than the nanosecond laser, and the silicon surface becomes rough, thus increasing the grid line pulling force. This article reports the changes in surface morphology under different conditions of UV-ps laser. The saturation current density of the laser processing area ($J_{0\text{laser}}$) measured by WCT120 was used to explore the laser damage and put forward the laser damage mechanism. Finally, the J_{sc} failure analysis of electroplated n-TOPCon solar cells was carried out.

2. Experimental Section

2.1. Solar Cells

All experimental pieces use n-type single crystal TOPCon solar cells with an area of 210 mm × 210 mm and a thickness of

170 μm . The precursor of TOPCon solar cells was prepared by using the standard preparation process of silicon wafers in the laboratory, as shown in **Figure 1a**. First, a random pyramid structure was prepared on the surface of the silicon wafer, and then the pn junction was formed by diffusion method. Then the ultra-thin SiO_2 and n-poly were prepared by low pressure chemical vapor deposition. The PSG on the front is removed with HF, and then the poly-Si layer is removed by wet etching process. After that, the AlOx was prepared on the front side of the solar cells by atomic layer deposition. Then, plasma enhanced chemical vapor deposition (PECVD) was used to deposit SiNx films on the front and back sides.

The front AlOx , the front and back SiNx layers are opened in air using an UV-ps laser. The frequency of the UV-ps laser is 2000 kHz, and the pulse time is 10 ps. The passivation layer on the front and back is opened by UV-ps laser for fast firing oven (FFO), which is used to recover the laser damage at high temperature. The wafer or sample surface was pretreated with HF for 30 s to remove the SiO_2 formed in the laser region. After pretreatment, nickel ($\approx 0.5 \mu\text{m}$), copper ($\approx 6 \mu\text{m}$), and silver ($\approx 0.5 \mu\text{m}$) were deposited by electroplating. The structure diagram of electroplated n-TOPCon solar cells is shown in **Figure 1c**. Where Ni is the seed layer to prevent Cu from spreading into silicon; Cu is the conductive layer, increasing the height of the grid line; and Ag is an anticorrosion layer that prevents copper oxidation and facilitates subsequent welding.

The laser fluence and overlap rate are changed by adjusting the laser power and speed. The observation of laser film opening by optical microscope shows that the laser fluence of 0.17, 0.18, 0.19 J cm^{-2} can realize the laser film opening completely, and there will be no over opening phenomenon (**Figure 1d**). Therefore, the effect of different laser fluences and different

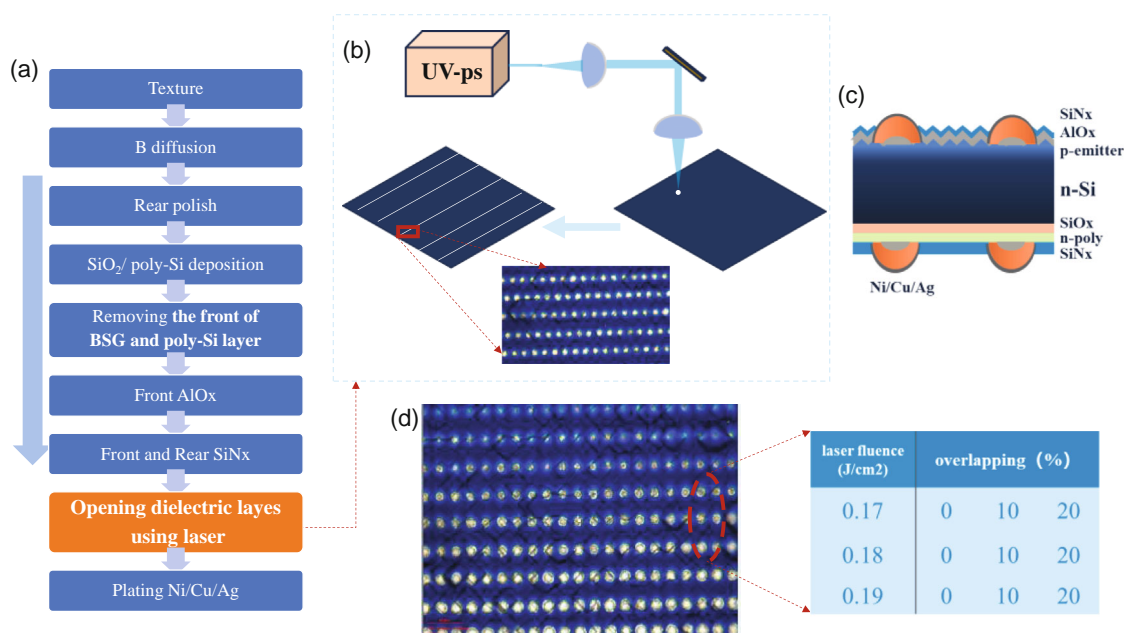


Figure 1. a) Process flow of n-TOPCon solar cell; b) simple diagram of laser action in dielectric layer; c) structure diagram of electroplated n-TOPCon solar cell; d) optical images representing the different surface morphologies after laser ablation (laser fluences from 0.14 to 0.22 J cm^{-2} with overlapping of 0%).

overlap rate on the performance of n-TOPCon solar cells and the study of laser etching mechanism were studied. The pn junction of n-TOPCon solar cells is on the front side, and the impact of the laser on the front side is greater than that on the back side.

2.2. Characterization Methods

The surface morphology of the contact opening by UV-ps was studied by optical microscope and scanning electron microscope. The film thickness, refractive index, and absorption coefficient of SiNx were measured by the ellipsometer (J.A. Woollam Co., Inc. M-2000XI). The reflectance of SiNx was measured by ultraviolet spectrophotometer (Lamabda 950). The influence of electrochemical differential capacitance voltage test (ECV model CVP 21) on the concentration distribution of B element doping after laser testing: the longitudinal concentration of B element was measured by secondary ion mass spectrometer (SIMS) after laser processing area. SintonWCT120 Test and evaluation of minority lifetime J0 laser: The changes of O element after laser film opening and HF pretreatment were analyzed by X-ray photoelectron spectroscopy (XPS). Loana tests the external quantum efficiency and the reflectivity of electroplated n-TOPCon solar cells.

3. Results and Discussion

If the photon energy matches the excitation energy of the material, the laser can be directly absorbed. The most important excitation mechanism is interband excitation, and the critical photon energy is determined by the bandgap.^[18] The SiNx layer used in this article is directly deposited by PECVD, with a refractive index of approximately $n = 2.1$ (Figure S1, Supporting Information). According to formula 1, the bandgap of SiNx is calculated to be ≈ 3.5 eV, as shown in the illustration in Figure 3. The bandgap of silicon is about 1.2 eV, and it takes three photons to pass through this bandgap. The photon energy of a laser with a wavelength of 355 nm is well matched with this bandgap energy, so it should be directly absorbed within the silicon nitride layer.^[19]

$$\begin{aligned} X &= 1240/\lambda \\ Y &= [\alpha \times (1240/\lambda)]^2 \end{aligned} \quad (1)$$

where λ is the wavelength (nm); α is the absorption coefficient.

As is well known that after laser irradiation, the vapor pressure of molten silicon increases, causing the dielectric layer on the silicon substrate to be removed from the lift caused by internal stress in the layer.^[8] It can be seen from Figure 2a that during the selective ablation process, the high local heating and rapid

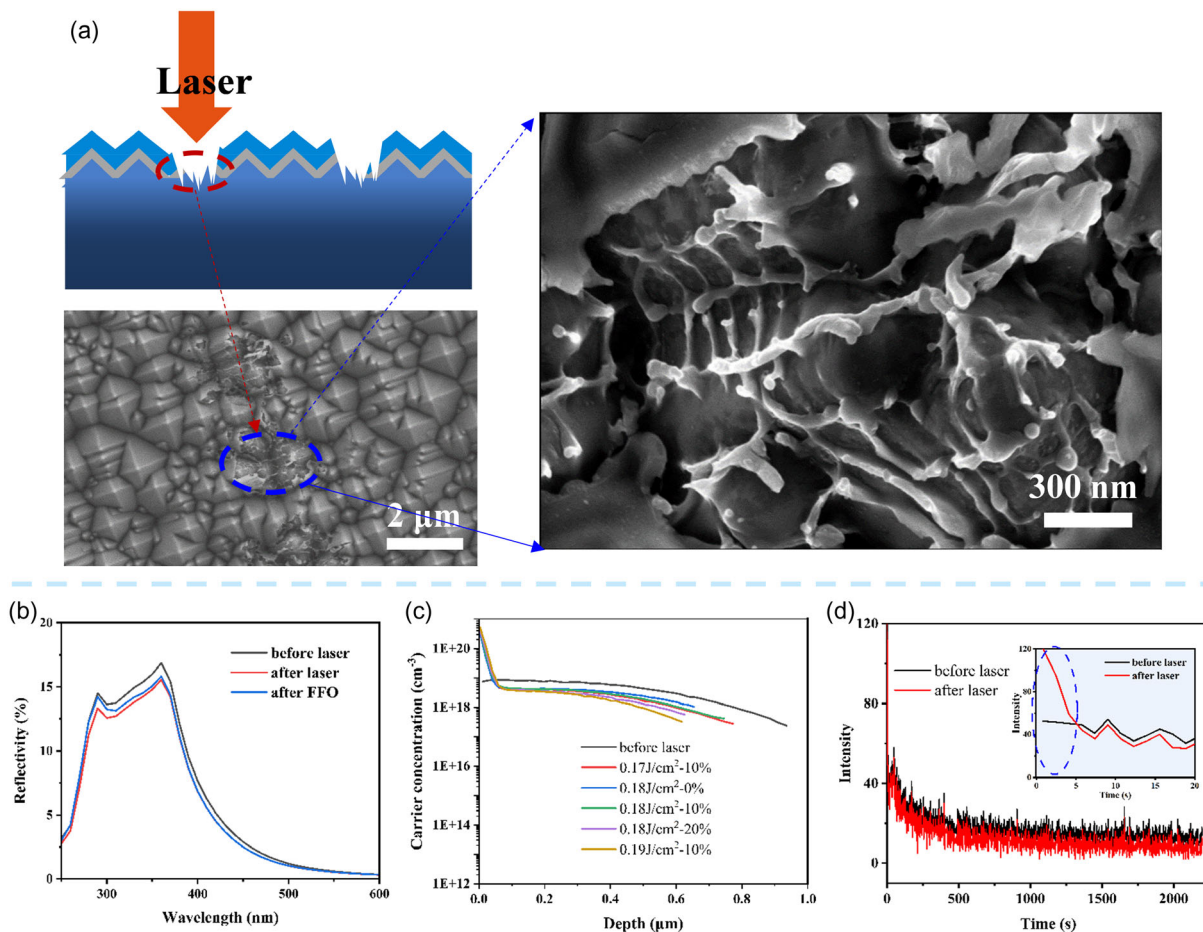


Figure 2. a) SEM view surface morphology after laser; b) the reflectance of SiNx before and after laser and FFO; c) ECV diagram of B element content under different laser fluences; d) SIMS diagram of longitudinal distribution of B element under 0.18 J cm^{-2} laser fluence and original sample.

cooling of the silicon will produce high thermal stress, causing the silicon surface to melt, become rough and melt, which may lead to defects. In order to study whether laser ablation will cause defects, the dielectric layer is ablated under different laser intensities. According to the experimental findings, the silicon surface will melt and exhibit extremely rough morphology. As can be seen from Figure S2, Supporting Information, silicon melting results in a very rough surface. The laser is focused from all sides on a very small volume at the top of the pyramid. Since heat deposition can only dissipate slowly from this small volume, silicon removal is inevitable. Although the laser is focused only from both sides in this case, the same effect occurs at the edge of the pyramid. Because the pyramid tip absorbs more energy from the laser beam, the melting state of the pyramid tip becomes more obvious.^[18] Consequently, under the same laser fluence, increasing the lasers spot overlap rate will increase the grating bonding force because of the increased surface roughness. However, as the overlap rate increases, the laser damage will increase accordingly (Figure S3, Supporting Information).

Reflectance measurements are performed on SiNx before and after laser ablation, as shown in Figure 2b. Amorphous silicon will form on the surface of SiNx after laser ablation, resulting in some modifications to the ultraviolet spectrum. However, amorphous silicon might reconsolidate or experience repairs to changes in the UV spectrum during the FFO.^[20] Two peaks are observed in the UV range of around 290 and 365 nm, even during high-throughput ablation (Figure S4, Supporting Information). These peaks are attributed to direct optical transitions in crystalline silicon. The peak at 290 nm is usually expected to be around 270 nm. This displacement is attributed to the response of the integrating sphere, which has a minimum response value of around 270 nm. Reflectivity measurements indicate that these defects cannot be attributed to the amorphization of the silicon surface, as the crystal structure of the surface appears to have been preserved after laser treatment.^[21]

During the process of laser ablation of the dielectric layer, the silicon beneath is heated and melted. Due to diffusion in the liquid is much faster than in the solid, the melting of silicon during the ablation process can cause significant changes in the emitter profile of the contact area. In order to study the change of emitter profile, we measure the change of element B concentration by ECV and SIMS, as shown in Figure 2c. The sudden increase of the carrier concentration after laser ablation of the dielectric layer may be due to the secondary doping effect of the B source in the high temperature environment generated by the laser. This is because the high temperature generated by the laser makes it easier for B-source atoms or molecules to migrate near the surface. The greater the laser fluence, the greater the damage to pn junction. The ECV curve is tested after the laser film is opened on the whole surface, and there will be no such damage in the actual production process.

In the region of $50\ \mu\text{m} \times 50\ \mu\text{m}$, the laser removes all SiNx (Figure S5, Supporting Information) and then performs SIMS test. As can be seen from Figure 2b, there is no difference between the emitter profile and the original profile, maintaining a similar tail shape. Due to the transient characteristics of the laser, almost no heat is diffused into the material, and the energy is completely used for ablation. This means that the melting of silicon is limited to the surface, and the surface profile of silicon

after laser ablation is retained.^[22] From the illustration of Figure 2d, it can be seen that the intensity of B element rises suddenly before the flight time is 5 s (consistent with the results of the first part of Figure 2c), indicating that the laser secondary doping of B element leads to the increase of the surface strength of B element. The SIMS and ECV tests show that the damage of laser to pn junction is minimal, and the laser damage can be further reduced by optimizing the laser parameters.

During the laser etching process, the laser pulse energy is absorbed by the silicon wafer, causing the electrons in the silicon wafer to be excited to a high energy state, and the dielectric layer begins to burn. If the initial number of conduction band electrons is high, there will be more excited electrons. The energy of these electrons exceeds the bandgap energy of the dielectric layer, so they migrate to the dielectric layer. In the case of low laser fluence, the laser pulse energy is directly absorbed by the dielectric layer. During the laser pulse duration, a high electron concentration is generated at the top of the dielectric layer, and these electrons absorb all the incoming photons. Therefore, only a few photons can reach the interface between the dielectric layer and the silicon layer.^[8] Because the laser pulse energy transmitted to silicon is too low, the dielectric layer cannot be removed. The high electron concentration causes the dielectric layer to heat up, which leads to the evaporation of the dielectric layer.^[23] As can be seen from the surface ablation model in Figure 3d, the laser pulse intensity in the center of Gaussian laser is higher than that in the outer ring, so the dielectric layer is partially ablated (Figure 3a). When the laser fluence reaches a certain threshold, the number of initially excited electrons increases, and these electrons can even absorb more photons, resulting in direct absorption and layer ablation of the medium after the end of the laser pulse (Figure 3b). When the laser fluence continues to increase, the silicon material will experience strong overheating conditions and begin to sublimate. At this time, the silicon material becomes thermodynamically unstable.^[24] After this, ablation occurs because of high speed nucleation of bubbles. When the thermal expansion coefficients of the Si and dielectric layer are different, and due to the high mechanical stress in the layer, gaseous silicon will cause the dielectric layer to expand and eventually cause the layer to break. As a result, the dielectric layer is completely removed (Figure 3c), with damage to its Si base.^[19] At different laser energy densities, a layer of heat-affected zone is formed in the c3 region of Figure 3d due to the resolidification of molten silicon, and its crystal structure is affected by amorphous and recrystallization.

The hypothesis of laser acting on the precursor of n-TOPCon solar cell is proposed according to the surface laser ablation model in Figure 3d. The light spot generated by the UV-ps laser used in this article is a Gaussian light spot, and its energy gradually weakens from the center to the edge. The laser intensity is high enough in the c1 region for the dielectric layer to absorb energy. The dielectric layer sublimates and SiO₂ forms on the surface as a result of some of the energy being absorbed by the silicon underneath and the dielectric layer. In the c2 region, the energy is not enough to sublimate the dielectric layer completely. At this time, the silicon substrate absorbs a lot of energy and melts, resulting in mechanical stress inside the dielectric layer, which lifts it from the surface and eventually ruptures. Because of the extremely low fluence in this area,

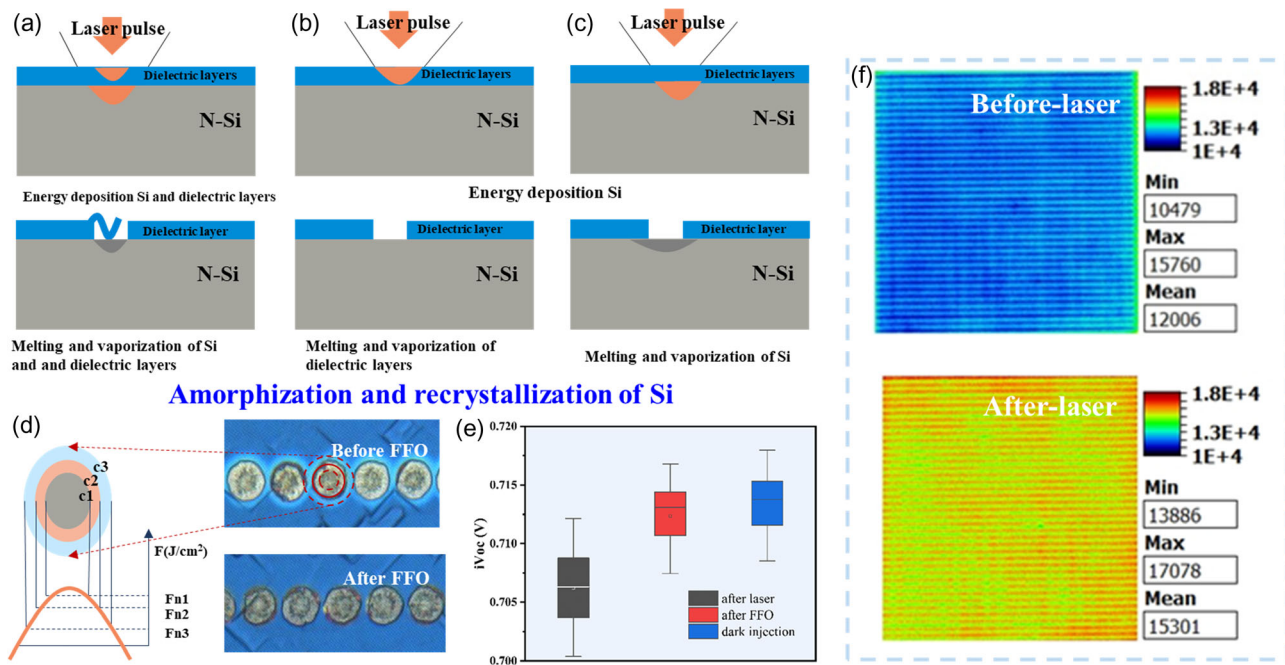


Figure 3. The SiNx dielectric layer in cross-section laser ablation a) less than the critical fluence threshold; b) critical fluence threshold; c) greater than the critical fluence threshold; d) surface laser ablation model, optical microscope image after laser treatment; before and after FFO; e) changes of n-TOPCon precursor $iVoc$; f) PL diagram.

the reoxidation process can happen, but it does so slowly. Since the fluence in region c3 is below the threshold, only silicon is able to absorb laser energy. As a result, not enough stress is created during the melting process to raise the upper dielectric layer. Silicon will transform into amorphous silicon during the quick cooling process.^[25]

When the sintering temperature exceeds 640 °C, the amorphous silicon will recrystallize (as shown in Figure 3), thereby repairing some of the damage caused by the laser. Illustration of Figure 3 show optical microscope images of ultraviolet picosecond laser openings film. The light blue area around the laser opening (as shown in Figure 3d of c3) is composed of amorphous silicon below the dielectric layer, which is caused by the rapid cooling of the Gaussian laser spot contour.^[26] When using a standard FFO process, most of the amorphous silicon is recrystallized, and the area appears dark blue again, which leads to a decrease in the recombination rate of the contact area.^[27] Figure 3e shows the $iVoc$ changes of n-TOPCon precursor before and after FFO. After high-temperature sintering, $iVoc$ increased by about 12 mV, which may be caused by the activation of passivation layer at high temperature. Finally, after dark injection, $iVoc$ increased by about 1 mV. Although the increase in $iVoc$ is not obvious, the minority carrier lifetime is improved at low injection concentration (carrier concentration of $1 \text{ E}^{15} \text{ cm}^{-3}$), as shown in Figure S6, Supporting Information. PL measurements further verify that high temperature sintering can repair some of the laser damage (as shown in Figure 3f). Under different laser fluxes and overlap rates, the results show similar repair effects (Figure S7, Supporting Information).

In summary, a standard FFO process is sufficient to recover some of the laser damage.

We employed a symmetrical structure sample with n-Si double-sided texturing, double-sided emitter, and passivation layer to analyze the recombination current in order to assess the impact of laser-induced defects on minority carrier recombination. The UV-ps laser is used to open different opening areas, as illustrated in Figure S8, Supporting Information. Each test sample contains 9 squares ($50 \text{ mm} \times 50 \text{ mm}$) in which the dielectric layer is opened by a laser with different open film areas. The boxes are labeled from 1 to 9 with a contact fraction of 0–2.2%.

The total recombination current ($J_{0\text{total}}$) is quantified by Sinton WCT120. The method proposed by Deckers et al.^[28] is used to extract $J_{0\text{laser}}$ in the laser ablation region. At high injection concentration ($5 \text{ E}^{15} \text{ cm}^{-3}$), $J_{0\text{total}}$ is the slope of $1/\tau_{\text{eff}}$, as shown in Formula 2. After neglecting for auger recombination, effective lifetime for the bulk (τ_{bulk}) does not change with changes in injection concentration.^[29] Therefore, $J_{0\text{open}}$ in the open film region and $J_{0\text{pass}}$ in the passivation region can be classified as $J_{0\text{total}}$. The relationship between $J_{0\text{total}}$ and the open film area is shown in Formula 3, in the absence of volume recombination and passivated surface recombination.^[30] Different contact fractions are opened on symmetric n-TOPCon structures using different laser fluence and overlapping (Figure 4a). The total recombination current density of $J_{0\text{total}}$ is measured with WCT120 at a carrier density of $5 \text{ E}^{15} \text{ cm}^{-3}$.

$$\frac{1}{\tau_{\text{eff}}} = \frac{1}{\tau_{\text{bulk}}} + J_{0\text{total}} \frac{N_D + \Delta p}{qn_i^2 W} \quad (2)$$

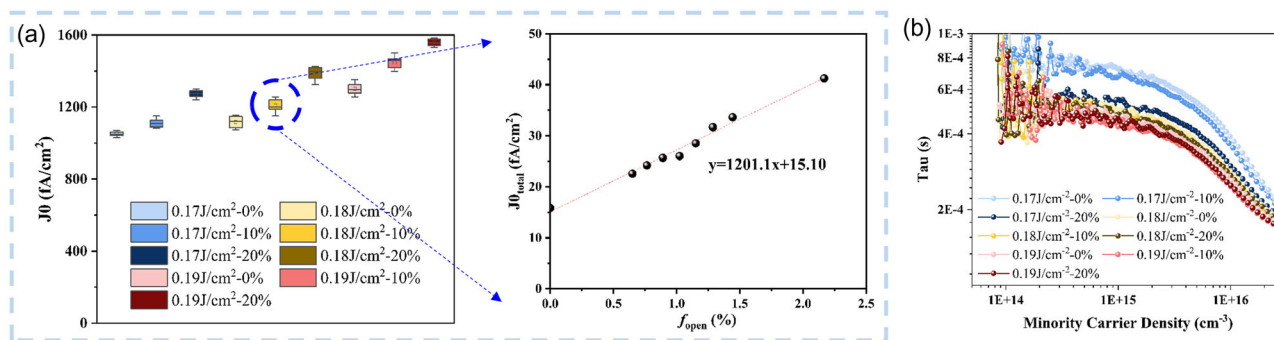


Figure 4. Local emitter saturation current density in the laser ablation region as a function of different laser fluxes and overlap rates a) $J_{0_{laser}}$ with different laser flux and overlap rate; The relationship between $J_{0_{total}}$ and f_{open} at 0.18 J cm⁻²-10% laser fluence; b) relationship between carrier concentration and minority lifetime at different laser fluence and overlapping.

$$J_{0_{total}} = 2J_{0_{pass}} + f_{open} (J_{0_{open}} - J_{0_{pass}}) \quad (3)$$

where τ_{eff} is the tested minority lifetime of each square; τ_{bulk} is the average body life; Δp is the average carrier concentration divided by the wafer thickness W ; q is the basic charge; n_i is the intrinsic carrier concentration; N_D is the based doping level.

The silicon nitride film layer is not entirely opened, despite the tiny $J_{0_{laser}}$ values for 0% and 10% overlap rates under 0.17 J cm⁻² laser fluence. This could result in poor adhesion between electroplating and make the gate line binding force of n-TOPCon Cell worse. Increasing the laser fluence and overlap rate will lead to an increase in the J_0 laser and will also cause more damage to the pn junction, thereby reducing the V_{oc} of the n-TOPCon solar cell, thereby reducing its efficiency.

Due to the double-sided symmetrical structure of the low-resistance sheet used, there will be errors in the $J_{0_{laser}}$ value, but the overall trend is consistent. The aforementioned information demonstrates that the dislocation produced by laser ablation can serve as a recombination center and that increasing the recombination brought on by laser ablation damage significantly shortens the silicon wafer's effective life (Figure 4b). The decrease in photoluminescence efficiency and the average minority carrier lifespan with increasing laser fluence can be ascribed to the rise in surface recombination velocity, which is directly linked to the rise in defect concentration in the vicinity of the surface. However, it can be speculated that these defects

are dislocations that appear at the interface between the melting zone and the body during the cooling process. In order to further confirm the nature and source of these defects, more in-depth exploration may be needed.^[31]

The model of laser-induced silicon oxidation is shown in Figure 5a. The growth mechanism of the oxide layer is similar to the formation of natural oxide SiO₂. In order to further grow the oxide layer, it is necessary for O₂ to diffuse into SiO₂ and hot electrons to escape from Si and pass through the SiO₂ layer to combine with O₂. Since the size of oxygen molecules is close to the volume of the lattice gap of the oxide layer, O₂ can diffuse in SiO₂. However, the lattice between silicon and silicon oxide does not match, so silicon electrons cannot directly pass through the oxide layer and combine with oxygen molecules to form a new oxide layer.^[32]

Under laser irradiation, hot electrons are produced in silicon. These hot electrons can penetrate the barrier layer and decompose oxygen molecules into atomic oxygen. Subsequently, some oxygen atoms and possible oxygen ions diffuse through the barrier layer until they reach the SiO₂ interface. Here, they react with silicon to form a SiO₂ layer.^[33] It should be noted that the formed SiO₂ layer is not conductive, which may affect the subsequent electroplating effect and the pull-off force of the gate line. Therefore, HF pretreatment is required before electroplating to remove the oxide layer formed during laser slotting.

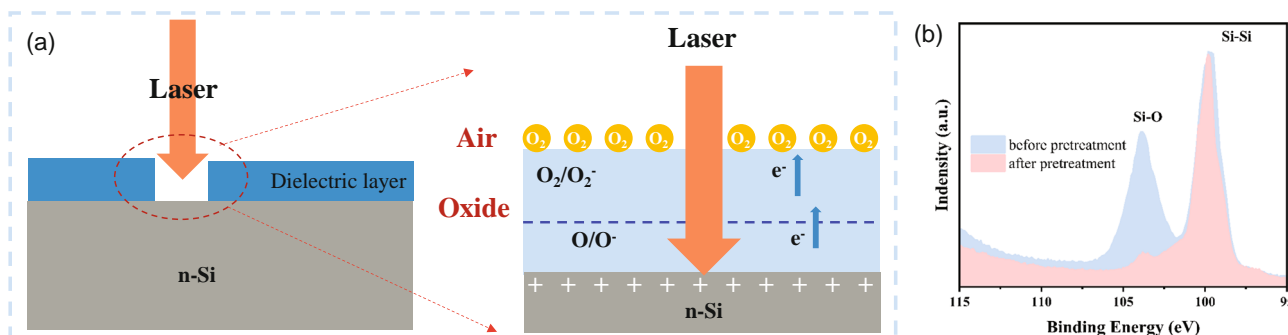


Figure 5. Schematic diagram of laser-induced oxide formation a) XPS diagram b) of Si 2p spectra in the laser open film region before and after pretreatment.

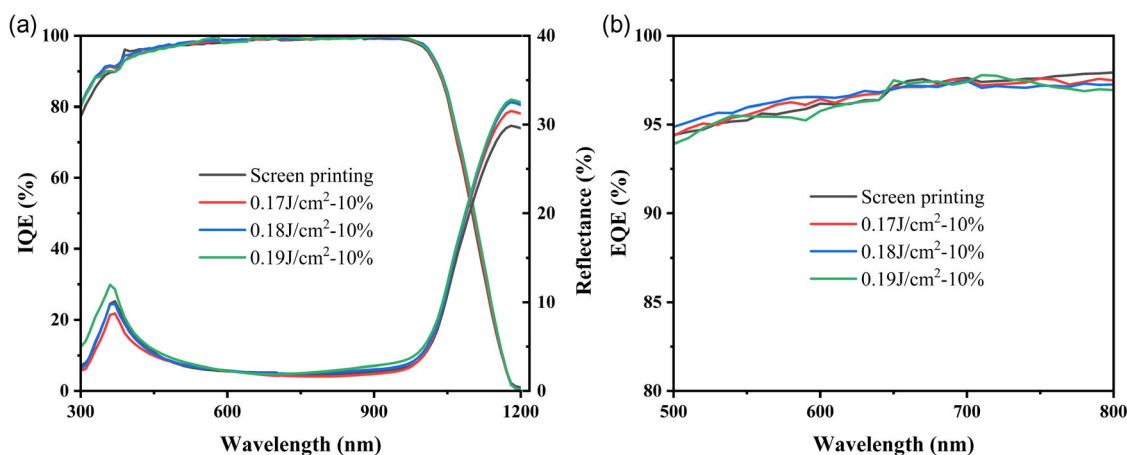


Figure 6. IQE diagram of electroplated and screen printed n-TOPCon solar cells under different laser flux conditions.

Figure 5b shows the $s2p^{3/2}$ XPS spectra of laser ablation of alkaline texture surface before pretreatment, with a peak of 99.3 eV being Si–Si bond and a peak of 103.3 eV being Si–O bond.^[15] Following pretreatment, the peak strength of the Si–O bond decreases rapidly, and the remaining Si–O bond may be the cause of the formation of natural oxides in the air. It is worth noting that during the experiment, the electroplating process will be carried out immediately after pretreatment, and the probability of the existence of natural oxide layer is negligible.

The J_{sc} losses of electroplated and screen printed n-TOPCon solar cells with different laser fluence are analyzed by IQE measurement. **Figure 6a** shows the IQE curves of electroplated and screen printed n-TOPCon solar cells under different laser flux conditions when the cell is operating under single-sun AM1.5 illumination. The J_{sc} loss mainly includes but is not limited to metal shading, loss caused by front surface reflection, poor light trapping loss (i.e., loss caused by long-wave light escaping from the front surface), and internal absorption loss (i.e., this part of light is absorbed by the solar cells but does not generate current). In the range of 500–800 nm wavelength, the characteristics of pn junction are reflected. As can be seen from **Figure 6b**, compared with SP, electroplating metallization has almost negligible damage changes to pn junction. The specific J_{sc} of losses are shown in **Table 1**. In the short wavelength range of 300–400 nm, J_{sc} of loss is mainly caused by metal shading and front surface reflection. The refractive index of electroplated n-TOPCon solar cells will

increase due to the improvement of SiNx reflectivity by pretreatment before electroplating (consistent with the test results in **Figure 2b**).

4. Conclusions

In this article, we studied the laser ablation opening of n-TOPCon precursor using UV-ps laser. In order to gain a deeper understanding of the ablation mechanism, we experimented with various combinations of laser energy and overlap parameters, and accordingly selected the best combination of laser parameters to minimize laser damage to the material. The optical and scanning electron microscopy were used to characterize the samples that had been laser-treated. The findings indicate a strong correlation between the laser-affected area's spatial distribution and the creation of these ablation surfaces. The dielectric layer can be fully opened by increasing the laser fluence and overlap rate, and the surface roughness can be increased by increasing the overlap rate under the same laser fluence. After laser ablation, the crystallinity of silicon in the heat affected zone on both sides of the groove area changes, which is mainly due to the amorphization caused by the interaction between the laser and the silicon material. After FFO, the heat-affected zone will disappear or be improved. By comparing the optical microscope images before and after FFO, we observed and confirmed these changes. These changes further improve the value of minority carrier lifetime and $iVoc$. The reflectance measurement shows that these defects cannot be attributed to the amorphization of the silicon surface because the crystal structure of the surface appears to be retained after laser treatment. Further research is needed to determine the nature of these defects. However, based on the existing evidence, we can reasonably speculate that these defects may be formed by dislocations at the interface between the melting zone and the bulk during the cooling process. According to the results of SIMS analysis, we found that the profile of the emitter did not change significantly compared with the original profile and maintained obvious kink and tail characteristics. Since the interaction between the laser and the material occurs in a very short time, almost no heat

Table 1. J_{sc} loss distribution for electroplated and screen printed n-TOPCon solar cells.

Sample	Lost due to poor light trapping [mA cm ⁻²]	Loss due to internal current loss issues [mA cm ⁻²]	Loss due to front reflectance and metal shading [mA cm ⁻²]
Screen-printed	0.81	0.83	1.62
Cu-plating- F_{th} 0.17 J cm ⁻² -10%	1.11	0.83	1.74
Cu-plating- F_{th} 0.18 J cm ⁻² -10%	1.08	0.68	1.86
Cu-plating- F_{th} 0.19 J cm ⁻² -10%	1.08	0.78	1.98

diffuses into the material, and the energy is completely used for ablation. Therefore, the melting of silicon is mainly limited to the surface, thus maintaining the profile of the emitter. Based on these results and material properties, we propose an ablation mechanism that depends on the partial lift on both sides.

The laser damage was evaluated by $J_{0\text{laser}}$. The results showed that both the increase of laser fluence and the increase of overlapping will increase the $J_{0\text{laser}}$. XPS analysis shows that laser slotting will produce oxide layer, which needs to be pretreated to remove SiO_2 , which is conducive to subsequent electroplating performance. The J_{sc} loss of electroplated n-TOPCon solar cells is mainly caused by the increase of the reflectivity of the front surface. High concentration doping will reduce laser damage, which can be studied in detail in the future. The next step will continue to discuss the effects of laser on different film thicknesses, bandgap dielectric layers, and so on.

Supporting Information

Supporting Information is available from the Wiley Online Library or from the author.

Acknowledgements

This work was supported by the Jiangsu Province Dual Carbon Technology Special Project (grant nos. BE2022022), Industry Outlook and Key Core Technologies in Jiangsu Province (BE2022022-4), the Natural Science Foundation of Jiangsu Province (grants no. BK20220240), and Qing Lan Project and 333 Project of Jiangsu Province.

Conflict of Interest

The authors declare no conflict of interest.

Data Availability Statement

Research data are not shared.

Keywords

ablation mechanism, n-TOPCon cell, surface damages, UV-ps laser

Received: October 23, 2023

Revised: April 10, 2024

Published online: May 15, 2024

- [1] X. W. Shen, P. C. Hsiao, Z. M. Wang, B. Phua, S. Lim, A. Lennon, *Sol. Energy Mater. Sol. Cells* **2022**, 240, 111638.
- [2] M. Pospischil, M. Kuchler, M. Klawitter, C. Rodríguez, M. Padilla, R. Efinger, M. Linse, A. Padilla, H. Gentischer, M. König, M. Hörteis, L. Wende, O. Doll, R. Zengerle, F. Clement, D. Biro, *Energy Procedia* **2015**, 67, 138.
- [3] X. Chen, K. Church, H. Yang, I. B. Cooper, A. Rohatgi, in *Proc., 37th IEEE Photovoltaic Specialists Conf. (PVSC)*, Seattle, WA, USA **2011**, p. 3667.
- [4] L. Kuang-Chieh, L. Yueh-Lin, L. Ming-Shiou, C. Chia-Chih, L. Chi-Chun, W. Chien-Chun, *Cu-plated Electrodes with Laser Contact Opening on n-type Crystalline Silicon Solar Cells*, Motech Industries, Inc, Tainan, Taiwan **2017**.
- [5] S. Singh, P. Choulat, J. Govaerts, A. Heide, V. Depauw, F. Duerinckx, R. Naber, M. Lenes, L. Tous, J. Poortmans, *Prog. Photovoltaics* **2022**, 8, 30.
- [6] B. Grubel, G. Cimiotti, C. Schmiga, V. Arya, B. Steinhäuser, N. Bay, M. Passig, D. Brunner, M. Glatthaar, S. Kluska, *IEEE J. Photovoltaics* **2021**, 3, 584.
- [7] M. Gebhardt, T. Kießling, M. Grimm, *LTJ* **2014**, 11, 18.
- [8] G. Heinrich, M. Bahr, K. Stolberg, T. Wütherich, M. Leonhardt, A. Lawrenz, *Energy Procedia* **2011**, 8, 592.
- [9] B. Grubel, G. Cimiotti, V. Arya, F. Feldmann, B. Steinhäuser, S. Kluska, M. Glatthaar, in *Proc., 36th European Photovoltaic Solar Energy Conf.*, Marseille, France **2019**, p. 1.
- [10] F. Feldmann, B. Steinhäuser, V. Arya, A. Büchler, A. Brand, S. Kluska, M. Hermle, S. Glunz, in *Proc., 33rd European Photovoltaic Solar Energy Conf. and Exhibition*, Munich Germany **2017**, p. 1.
- [11] B. Grubel, G. Cimiotti, C. Schmiga, V. Arya, S. Kluska, *IEEE J. Photovolt* **2021**, 99, 1.
- [12] M. S. Trtica, B. M. Gakovic, B. B. Radak, D. Batani, T. Desai, M. Bussoli, *Appl. Surf. Sci.* **2007**, 254, 1377.
- [13] G. Heinrich, I. Hşger, M. B. Şhr, K. Stolberg, T. W. Ytherich, M. Leonhardt, A. Lawrenz, G. Gobsch, *Energy Procedia* **2012**, 27, 491.
- [14] L. Wang, X. Huang, J. Lv, J. B. Wang, M. Cao, T. Wang, J. P. He, *J. Electron. Mater.* **2023**, 52, 3859.
- [15] X. Shen, P. C. Hsiao, B. Phua, A. Stokes, *Sol. Energy Mater. Sol. Cells* **2019**, 205, 110285.
- [16] C. Dang, R. Labie, E. Simoen, J. Poortmans, *Energy Mater. Sol. Cells* **2018**, 184, 57.
- [17] A. Lennon, J. Colwell, K. P. Rodbell, *Prog. Photovoltaics Res. Appl.* **2019**, 27, 67.
- [18] A. Knorz, M. Peters, A. Grohe, C. Harmel, R. Preu, *Prog. Photovoltaics* **2009**, 17, 127.
- [19] G. Heinrich, A. Lawrenz, *Sol. Energy Mater. Sol. Cells* **2014**, 120, 317.
- [20] A. Straub, P. I. Widenborg, A. Sproul, Y. Huang, N. Harder, A. G. Aberle, *J. Cryst. Growth* **2004**, 265, 168.
- [21] G. Poulain, D. Blanc, A. Focsa, M. De Vita, K. Fraser, Y. Sayad, M. Lemiti, *Mater. Sci. Eng. B* **2013**, 178, 682.
- [22] A. Knorz, M. Aleman, A. Grohe, R. Preu, S. W. Glunz, in *European Photovoltaic Solar Energy Conf.*, Hamburg, Germany **2009**.
- [23] K. Sokolowski-Tinten, J. Bialkowski, D. von der Linde, *Phys. Rev. B* **1995**, 51, 186.
- [24] K. Sokolowski-Tinten, J. Bialkowski, A. Cavalleri, D. von der Linde, *Phys. Rev. Lett* **1998**, 81, 224.
- [25] C. Molto, J. E. Leeb, J. Nekardad, V. Aryad, S. Bechu, M. Bouttemyc, A. Etcheberry, E. Drahi, P. P. Grand, A. M. Goncalves, *Sol. Energy Mater. Sol. Cells* **2019**, 202, 110149.
- [26] N. Bay, A. A. Brand, A. Biichler, *Energy Procedia* **2017**, 12, 823.
- [27] J. Bonse, *Appl. Phys. A* **2006**, 84, 63.
- [28] J. Deckers, X. Loozen, N. Posthuma, B. O'Sullivan, M. Debucquoy, S. Singh, M. Aleman, M. Recaman, I. Gordon, P. Verlinden, R. Mertens, J. Poortmans, in *Proc., 28th European Photovoltaic Solar Energy Conf. and Exhibition* **2013**, p. 806.
- [29] A. Cuevas, *Sol. Energy Mater. Sol. Cells* **1999**, 57, 277.
- [30] C. Dang, R. Labie, L. Tous, R. Russell, M. Recaman, J. Deckers, A. Uruena, F. Duerinckx, J. Poortmans, *Energy Procedia* **2014**, 55, 649.
- [31] J. Chen, J. Deckers, P. Choulat, I. Kuzma-Filipek, M. Aleman, U. D. C. Angel, Z. R. Du, F. Duerinckx, B. Hoex, J. Szlufcik, *Prog. Photovoltaics* **2015**, 23, 1706.
- [32] Z. R. Du, C. T. Zhang, F. P. Li, R. Zhou, M. H. Hong, *IEEE J. Photovoltaics* **2016**, 6, 617.
- [33] A. Büchler, S. Kluska, F. Meyer, A. A. Andreas, J. Bartsch, M. Glatthaar, *Sol. Energy Mater. Sol. Cells* **2017**, 166, 197.